ANL/CHM/CP--87532
CONF-9510119--5

Submitted to: *Reviews of Scientific Instrumentation*



SEPTEMBER 25, 1995

# ANOMALOUS SMALL ANGLE X-RAY SCATTERING STUDY OF LAYERED SILICATE CLAYS CONTAINING NI(II) AND ER(III)

P. THIYAGARAJAN*, K.A. CARRADO, S.R. WASSERMAN, K. SONG AND R. E. WINANS

INTENSE PULSED NEUTRON SOURCE DIVISION* AND CHEMISTRY DIVISION, ARGONNE NATIONAL LABORATORY, ARGONNE, IL 60439



*Author to whom all correspondence should be addressed.
(708) 252-3593.

# Anomalous Small Angle X-ray Scattering Study of Layered Silicate Clays Containing Ni(II) and Er(III)

**P. Thiyagarajan*, K.A. Carrado, S.R. Wasserman, K. Song, and R. E. Winans**

Intense Pulsed Neutron Source Division* and Chemistry Division, Argonne National Laboratory, Argonne, IL 60439

## Abstract

These studies concern the synthesis of heterogeneous catalysts and the incorporation of heavy metals in trapping media. The Ni(II) containing clays were synthesized at 200°C whereas those containing Er(III) were ion-exchanged natural clays. For the first system, ASAXS data were measured at 5 different energies near the Kα edge of Ni at three different reaction times: unreacted, 4 hrs, and 15 hrs, when the crystallization is essentially complete. The data for the unreacted sample showed no correlations for a lamellar particle, while that reacted for 4 hrs indicated the evolution of lamella, and the crystallized sample (15 hrs) exhibits much larger lamellar correlations. Systematic variations are seen in the data for the 4 hr and 15 hr samples that are due to the anomalous scattering from the ordered Ni atoms in the layered silicates. The erbium study provides the first scattering measurements of heavy metal ion solvation and migration in clays, which has implications for both catalysis and environmental issues. Systematic energy-dependent variations in the signals near the $L_{III}$ edge of Er are observed for the hydrated sample, but not for the "dry", as-prepared sample.

## I. INTRODUCTION

Smectite clay minerals are layered metal silicates whose sheets can swell to incorporate up to several layers of water molecules. Each sheet is made up of one octahedral metal oxide layer, usually aluminum or magnesium, that is sandwiched by two tetrahedral silicate layers. Isomorphous substitutions within this framework give rise to a net negative charge on the lattice that is compensated for by the presence of exchangeable ions within the hydrated interlayer.[1] Clays have a long history of applications as catalysts, catalyst supports, adsorbents, ion-exchangers, etc., many of which have an environmental relevance.[2]

Clay minerals can incorporate heavy metal ions both within the lattice framework and between the interlayer regions. Each situation has relevance to a particular application, and we will examine one example from each case in this paper. The first involves the formation of a Ni-silicate clay which has shown potential as a hydroisomerization and hydrocracking catalyst.[3] In this case the nickel ions exist within the clay lattice framework in the octahedral sheet (Fig. 1). In the second example, a clay ion-exchanged with Er(III) ions, which therefore exist in the interlayer region (see Fig. 1), is examined in hydrated and non-hydrated forms. This has relevance to the structure, migration, and reactivity of the sites active during ion-exchange of hazardous heavy metal ions.

Small angle X-ray scattering (SAXS) has numerous applications in chemistry, metallurgy, biology, polymer science, and colloidal systems.[4] It examines correlations at distances from 10 to 1000 Å and provides information about the size, morphology, and interactions of a system of particles or pores in solution or the solid state (references). SAXS can also be used to follow the phase transitions, crystallization, and aggregation within a system.

The SAXS intensity as a function of the wave vector is due to the distance correlations of all the atoms in the particles of interest. Anomalous small angle X-ray scattering (ASAXS) refers to extensions of standard SAXS experiments in which the energy of the probing X-rays are tuned near the absorption edge of an element in the sample.[5,6] By performing SAXS experiments near the characteristic absorption edge of any given atom, it is possible to vary the contrast for scattering of

that particular element.[7,8] This systematic variation in contrast yields the partial scattering functions of the specific atomic species. In general, the atomic scattering can be expressed as:

$$f(q,E)=f_0(q) + f'(q,E) + if''(q,E) \qquad (1)$$

where E is the energy of the probing X-rays and q is the momentum transfer ($q=4\pi\sin\theta/\lambda$, where $2\theta$ is the scattering angle and $\lambda$ is the wavelength of X-rays). The parameters f' and f'' are the real and imaginary parts of anomalous dispersion. They each vary sharply at energies within 10 eV of the absorption edge. The imaginary scattering factor, f'', represents the absorption of X-rays which results in photoemission of a core electron. Variation in f' is responsible for the change in contrast seen in ASAXS signals.[5] These two quantities are related by the Kramers-Kronig relation. Typically f' is determined by measuring the energy-dependent absorption spectrum, f'', and applying the Kramers-Kronig transformation. Near the absorption edge of a given atom the scattering intensity, I, varies as a function of energy or wavelength (equation 2).[9]

$$I(q,\lambda) = I_0(q) + f'(\lambda)I_C(q,\lambda) +[f'^2(\lambda) + f''^2(\lambda)]\, I_R(q) \qquad (2)$$

Here $I_0$ represents the nonresonant, energy-independent scattering. The cross term, $I_C$, reflects scattering between the specific element of interest and the remainder of the material, while $I_R$ corresponds to the distance correlations of just the resonant scatterers.

Since f' and f'' are sharply varying functions near the edge, these experiments require the highest possible energy resolution (of the order of $\Delta\lambda/\lambda=10^{-4}$) for the probing monochromatic X-rays. In these experiments we determine the small angle scattering using incoming X-rays with 4 to 5 different energies. All but one of these energies are near the absorption edge of the atom of interest. The last measurement, using X-rays whose energy is 150 eV below the edge, gives a direct measurement of the nonresonant scattering, $I_0$, since at this energy f' and f'' are effectively zero. From these sets of data, in principle one can obtain a set of 3 to 4 differential scattering data after the subtraction of $I_0$. If the SAXS data as a function of energy are placed on an absolute scale, one can then use f' and f'' values to obtain the partial structure factors, $I_C$ and $I_R$, by least square analysis. The maximum variation in the SAXS signals near the edge depends on the maximum value of the

variation of f' for a given atom. In general, the variation of f' is larger near the $L_{III}$ edges than for the K edges. Therefore, if a transition metal ion is of interest, generally a larger weight % is necessary.

The SAXS technique is quite useful for following the evolution of layered structures as a function of reaction time. The ASAXS technique can reveal the distribution of specific metallic species within a matrix. We have used SAXS to examine the general mechanism of formation of layered particles while simultaneously using ASAXS to obtain species-specific information in these materials. We have also used ASAXS to examine the distribution of heavy ions within the interlayer of a natural clay mineral.

## II. EXPERIMENTAL

The incorporation of Ni ions within the layered framework is accomplished by following the method of Mizutani et al.[10] In this preparation, 2.07 gm $Na_4SiO_4$ is dispersed in 200 ml DDW, to which is added 20.4 ml 2N HCl to pH 3 .0. Then 1.07 gm $NiCl_2 \cdot 6H_2O$ are added, followed by 41 ml 1N NaOH at a rate of 0.2 ml/min. The light-green gel is then placed in an autoclave for heating at 200°C for various times, then centrifuged, washed, dried at 100°C, and powdered. Bentolite L, a natural $Ca^{2+}$-bentonite that has been purified to removed all but 0.2 wt% Fe impurities, was obtained from Southern Clay Products. This was ion-exchanged with Er(III) ions by stirring 1 gm clay in 100 ml of 0.1M $ErCl_3 \cdot 6H_2O$ overnight, followed by centrifugation, washing, and drying at room temperature. X-ray powder diffraction patterns were obtained on a Scintag PAD V instrument with Cu $K_\alpha$ radiation; samples were held as loosely packed powders in a horizontally mounted sample tray.

The powder samples were contained in a cell with kapton windows for SAXS measurements. The samples were measured at SAXS beamline BL 4-2 at the Stanford Synchrotron Radiation Laboratory in Stanford, CA.[11] This beamline has a platinum coated mirror which focuses the X-rays in the horizontal direction. A 62 μRad slit upstream from this mirror defines the energy resolution of the probing X-rays at <2 eV. The reflected beam from the mirror is monochromated by a double-

crystal Si(111) monochromator. The cross-sectional area of the X-ray beam, 3 mm x 1 mm, is defined by two guard slits. The beam was focused at a 20 cm long 1-dimensional position sensitive gas detector. The sample was located approximately 2.2 m upstream to the detector. Two ionization chambers, one before and one after the sample, monitored the intensity of the incident and absorbed X-rays. These monitors were also used to determine the absorption edge for Ni or Er in each of the samples. The entire beam path was under vacuum except at the sample. In this configuration the SAXS instrument can measure data in the q region from 0.008 to 0.25 $Å^{-1}$.

The acquisition time for each scattering profile was 5 minutes. During the acquisition of the scattering data, the energy of the incoming X-rays was cycled through each of the energies for 5 to 10 cycles, depending on the desired statistical precision. This procedure aided in the assessment of the stability of the sample, as well as the position of the X-ray beam. For Ni-clays, the ASAXS data was collected at 8089, 8319, 8327, 8331, and 8333 eV. The last energy is that of the nickel edge. For Er-clays, an absorption edge at 8372.6 eV corresponding to the $L_{III}$ edge of Er(III) was found. The ASAXS for the powder samples were then measured at 8100, 8355, 8368, 8370 and 8372 eV. The measurements were made for 5 minutes at each energy for 5 to 10 cycles depending on the required statistical precision.

## III. Results and Discussion

*Synthesis of Ni-Containing Clays*

Modified Guinier analysis was used to extract the correlations for the sheet-like particles expected during the formation of layered structures. This approach is based on the fact that the intensity of scattering for infinitely large sheets varies as $q^{-2}$.[4] When a Guinier analysis is performed by plotting $\ln[q^{-2} \cdot I(q)]$ as a function of $q^2$, a linear region indicates the presence of sheet-like particles. The negative slope contains information about the thickness factor, $R_t$, of the sheets as seen in equation 3.

$$I_{sheet}(q) = q^{2} \cdot \exp(-q^{2} \cdot R_t^{2}) \qquad (3)$$

In addition, the lowest $q^2$ value at which the curve starts to decrease yields qualitative information on the aspect ratio of the sheets. If such a plot does not contain any linear region with a negative slope, then the system does not contain any sheet like particles. In these experiments the thickness factor ($R_t$) can be measured in a q-region such that $q \cdot R_t < 0.8$. The thickness of the sheet is equal to $\sqrt{12} \cdot R_t$. Figure 2 shows a modified Guinier plot for the sample of unreacted clay. In the region where $q^2 > 0.001$ $A^{-2}$ there are no sheet-like correlations indicated. The steeply rising lowest $q^2$ region ($q^2 < 0.001$ $A^{-2}$) in this plot is due to the strong scattering from the various interfaces in the reactants, and does not correspond to sheets. Modified Guinier plots of the ASAXS data for a powder sample prepared after a reaction time of 4 hrs (Figure 3), on the other hand, do have negative slopes indicating the presence of layered particles. The slopes for the curves collected at the 5 different energies are similar. The deduced thickness from these slopes is 28.8 ± 0.9 Å. The decrease with increasing energy of the y-intercept values from these 5 curves are due to the variation of the f' value of Ni.

The X-ray powder diffraction (XRD) pattern of this sample is shown as an inset to Figure 3. It not only confirms the presence of layers, but also shows that a fairly well crystallized sample exists after just 4 hrs of reaction time. The basal, or d(001), spacing occurs at about 11Å, although the SAXS data indicate a larger layer thickness of 28.8 Å. The SAXS data apparently reflect the average thickness of the aggregated particles as they form, while the powder diffraction measures the interlayer spacing of the aluminosilicate sheets.

After a reaction time of 15 hrs, the slope of the Guinier plot changes significantly (Figure 4). In addition, the lowest $q^2$ value at which the linear curves start decreasing is much lower for the 15 hr sample than for the 4 hr sample, implying a larger aspect ratio of the layered particles. The larger slope for the 15 hr sample corresponds to a thickness of 48.1±0.3 Å. The variation of these signal intensities as a function of the energy of the X-rays indicates the presence of Ni-Ni correlations in the layered particles (see Fig. 1). Were nickel ions to remain in solution, there would be no order and therefore no specific, observable Ni-Ni correlations. The observable changes in intensity (ASAXS)

for the unreacted sample are due to the fact that Ni exists here as $Ni(OH)_2$. The XRD pattern shows sharper peaks, indicating the longer-range crystalline order that was deduced from the ASAXS investigation, and a d-spacing of 10 Å.

*Ion-Exchanged Er(III)-Clays*

In order to examine how the distribution of metal ions (labels) changes as solvent is added to a clay interlayer, we introduced erbium(III) cations by standard ion-exchange techniques. A lanthanide ion was used because the metal loading in an ion-exchanged clay are on the order of only a few weight %. Dry and wet samples of this material were examined using ASAXS and XRD. Figure 5 presents the ASAXS modified Guinier plots and the powder diffraction data for dry sample of Er-clay. The X-ray diffraction pattern corresponds to a (001) interlamellar spacing of 15.0 Å. The modified Guinier analysis yields a thickness of 52 ±1 Å for the clay particles. Unlike the Ni-containing synthetic clays (Fig. 4), the curves in Figure 5 do not tend to decrease in the low $q^2$ region. This natural clay has a larger aspect ratio than the synthetic material discussed above. As the energy of the X-rays is changed, there is no variation in the intensity of scattering. This result implies that the Er(III) ions are not located at specific, regularly ordered sites on the clay lattice.

The ASAXS data for the Er-clay sample after addition of excess water are shown in Figure 6. This figure also contains the X-ray powder diffraction pattern with an increased d-spacing of 19.5Å. Unlike the "dry" sample (Fig. 5), the ASAXS signals for the wet sample systematically vary as a function of the incident X-ray energy. The signal intensity decreases as the absorption edge of erbium is approached. This result indicates that there are correlations between Er(III) cations in the swelled clay which are not present in the dry material. ASAXS thus gives unique information about the ability of the solvent (water) to solvate Er(III) ions within the clay interlayer. More experiments will be done to elucidate why the correlations are not observed for the dried material.

## IV. Conclusions

We have demonstrated the usefulness of the ASAXS technique to the characterization of two important systems in materials chemistry. The evolution of a synthetic clay containing Ni atoms has been monitored with ASAXS, and the systematic variation of the signal intensity as a function of energy near the Ni edge clearly demonstrate the incorporation of Ni in the lamellar lattice. In the case of ion-exchanged clays, ASAXS adds unique insight into the role of solvent in promoting the interaction of ions, at least lanthanide ions, within a silicate clay interlayer environment. This complements the short-range information that has been obtained for Cu(II) ions during solvation in a clay by X-ray absorption spectroscopy.[12]

**Acknowledgments.** This work was performed under the auspices of the Division of Chemical Sciences, Office of Basic Energy Sciences, U. S. Department of Energy, under contract number W-31-109-ENG-38. Research at SSRL is supported by the Department of Energy, Office of Basic Energy Sciences. We also thank H. Tsuruta for assistance with BL-4-2 at SSRL, and S. E. Yuchs for the powder diffraction pattern of the wet Er-clay sample.

## References


[1]R. E. Grim, *Clay Mineralogy* (McGraw-Hill, NY, 1968).

[2]A. C. D. Newman, *Chemistry of Clays and Clay Minerals* (Mineralogical Society, London, 1987).

[3](a) J. J. L. Heinerman, I. L. C. Freriks, J. Gaaf, G. T. Pott, J. G. F. Coolegem, *J. Catal.* **80**, 145 (1983); (b) H. E. Swift, in Advanced Materials in Catalysis, edited by J. J. Burton and R. L. Garten (Academic Press, NY, 1977), p. 209.

[4]O. Glatter and O. Kratky, in *Small Angle X-ray Scattering* (Academic Press, NY, 1982).

[5]H.B. Stuhrmann, *Quarterly Rev. Biophys.* **14**, 433 (1981).

[6]J.E. Epperson and P. Thiyagarajan, *J. Appl. Cryst.* **21**, 652 (1988), and references therein.

[7]R.C. Miake-Lye, S. Doniach, K.O. Hodgson, *Biophys. J.* 287 (1983).

[8]M. J. Regan, M. Rice, M. B. Fernandez van Raap, A. Bienenstock, *American Crystallographic Association Meeting Abstracts*, (Montreal, QE, 1995), p. 64.

[9]O. Kuhnholz, *J. Appl. Cryst.* **24**, 811 (1991).

[10]T. Mizutani, Y. Fukushima, A. Okada, O. Kamigaito, *Bull. Chem. Soc. Jap.* **63**, 2094 (1990).

[11]S. Wakatsuki, K. O. Hodgson, D. Eliezer, M. Rice, S. Hubbard, N. Gills, S. Doniach and U. Spann, *Rev. Sci. Instrum.* **63**, 1736 (1992).

[12]K. A. Carrado and S. R. Wasserman, *J. Am. Chem. Soc.* **115**, 3394 (1993).

## Figure Captions

Figure 1. Dark circles represent nickel ions within the silicate lattice on the left, and dark circles represent erbium ions within the interlayer space on the right.

Figure 2. Modified Guinier sheet analysis of the ASAXS data for the unreacted powder of the Ni-containing synthetic clay. ASAXS data were measured at 5 energies as discussed in the text.

Figure 3. Modified Guinier sheet analysis of the ASAXS data for the Ni-clay after 4 hrs of reaction time. The fitted lines with a negative slope indicate the evolution of layered particles; the powder diffraction data is also shown.

Figure 4. Modified Guinier sheet analysis of the ASAXS data for the Ni-clay after 15 hrs of reaction time; the powder diffraction data is also shown.

Figure 5. Modified Guinier sheet analysis of the ASAXS data for the "dry" Er(III)-clay powder displaying 4 of the energies measured near the $L_{III}$ edge of Er. The inset shows the powder diffraction data.

Figure 6. Modified Guinier sheet analysis of the ASAXS data for the "wet" Er(III)-clay powder displaying 3 of the energies measured near the $L_{III}$ edge of Er. The inset shows the powder diffraction data.

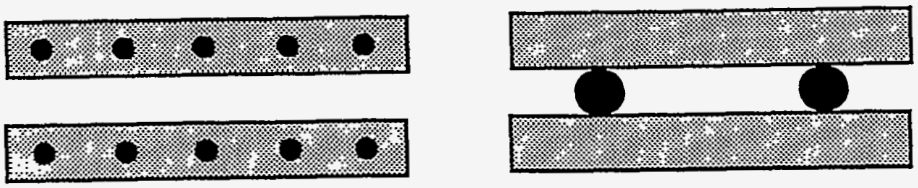

Figure 1

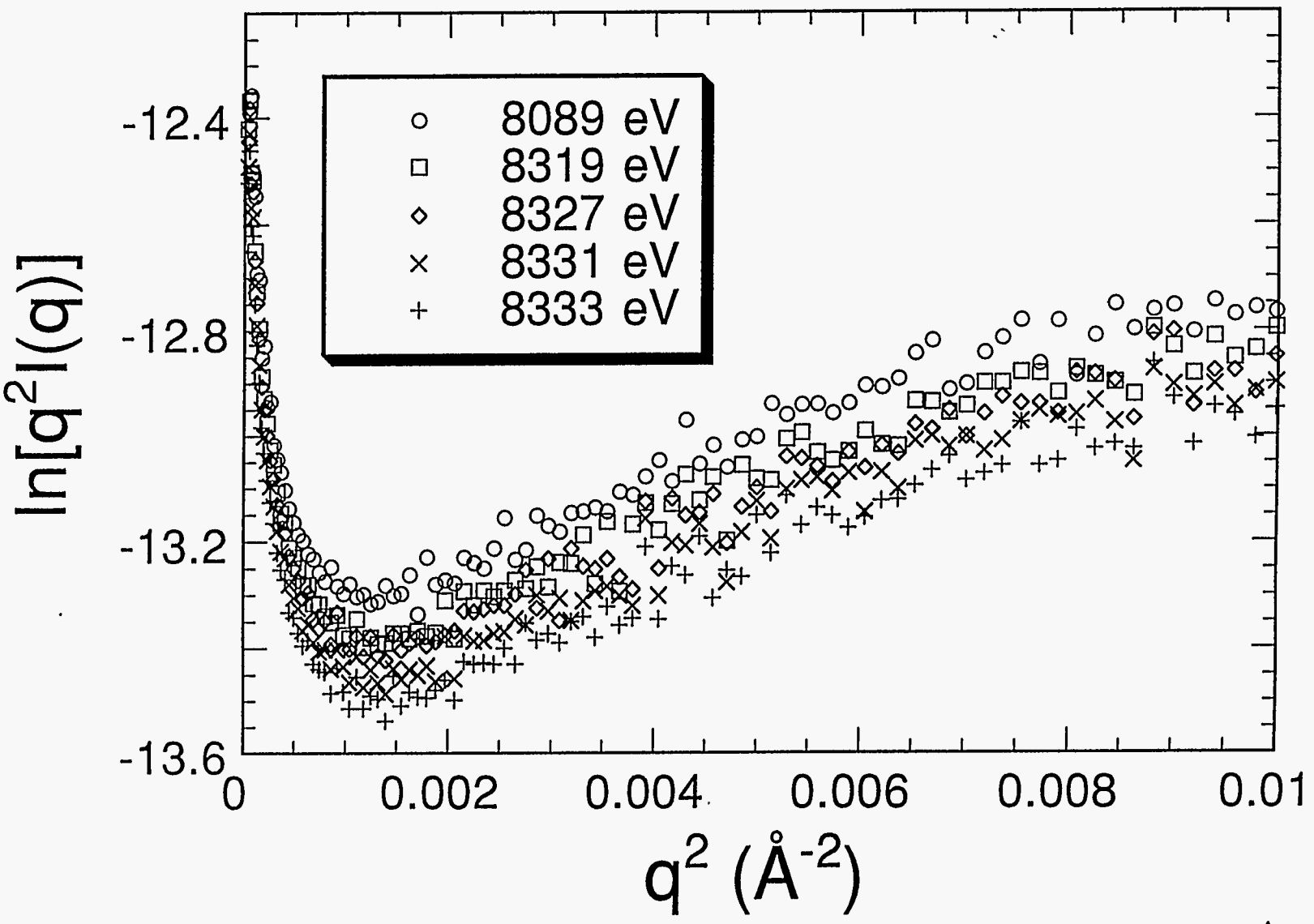
8089 eV
8319 eV
8327 eV
8331 eV
8333 eV
-12.4
-12.8
-13.2
-13.6
0
0.002
0.004
0.006
0.008
0.01
ln[q²I(q)]
q² (Å⁻²)

Figure 2

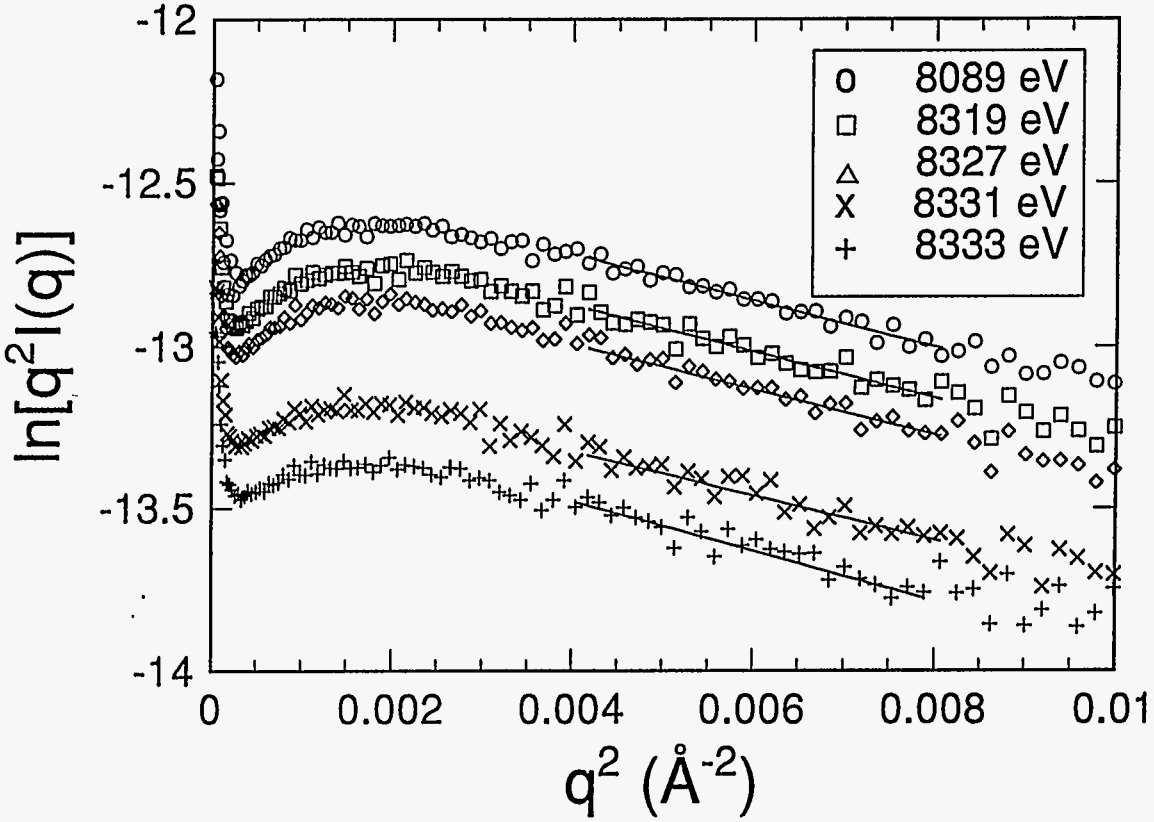
-12
-12.5
-13
-13.5
-14
0
0.002
0.004
0.006
0.008
0.01
ln[q²I(q)]
q² (Å⁻²)
o 8089 eV
□ 8319 eV
△ 8327 eV
X 8331 eV
+ 8333 eV

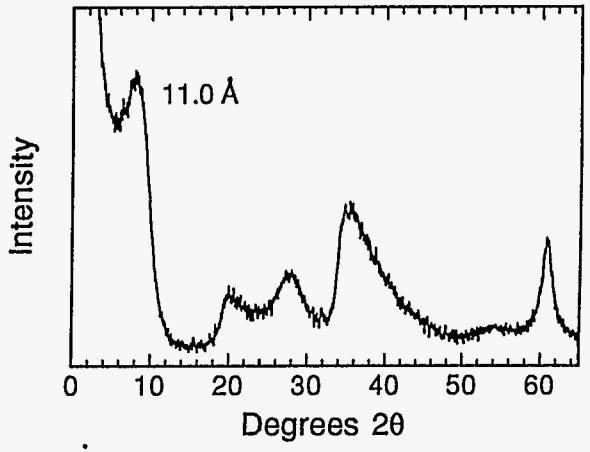
11.0 Å
Intensity
0
10
20
30
40
50
60
Degrees 2θ

Figure 3

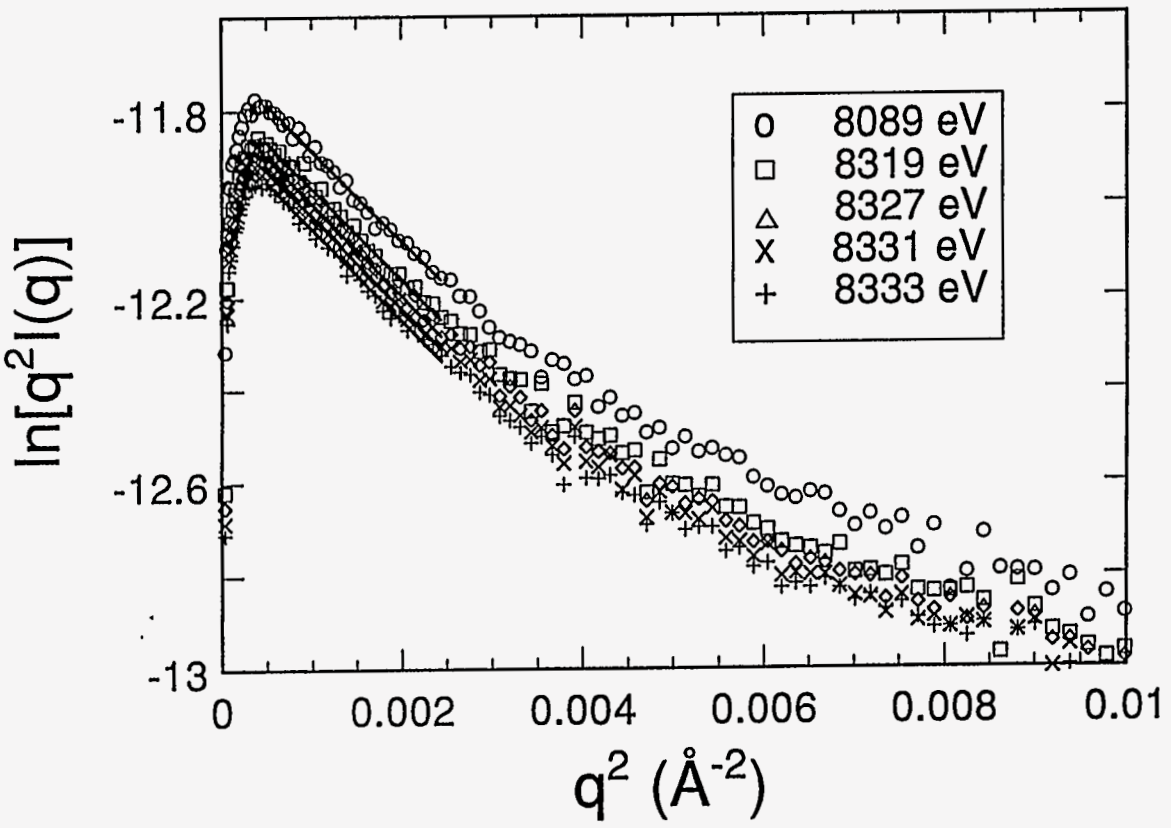
ln[q²I(q)]
-11.8
-12.2
-12.6
-13
0
0.002
0.004
0.006
0.008
0.01
q² (Å⁻²)
o 8089 eV
□ 8319 eV
△ 8327 eV
X 8331 eV
+ 8333 eV

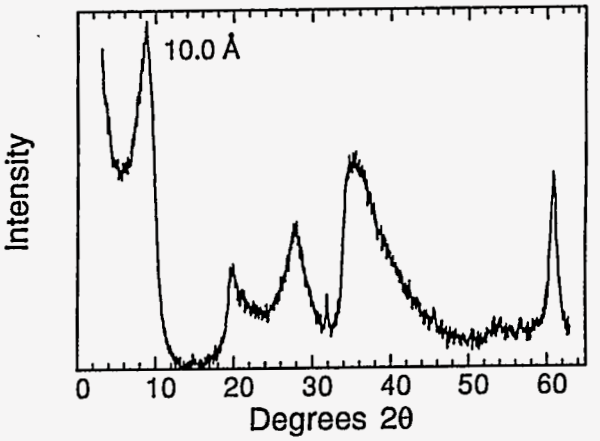
Intensity
10.0 Å
0
10
20
30
40
50
60
Degrees 2θ

Figure 4

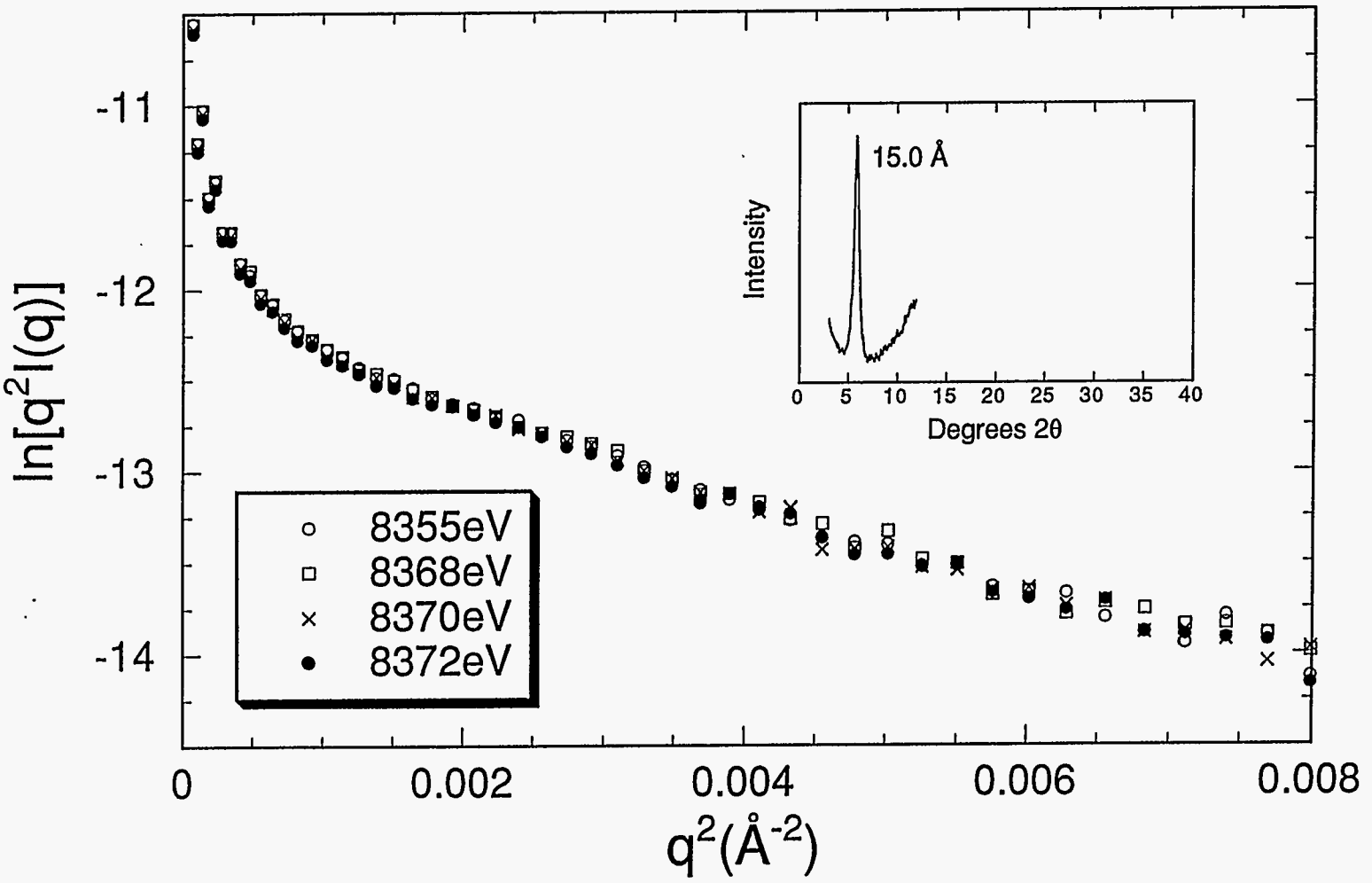
-11
-12
-13
-14
ln[q²I(q)]
0
0.002
0.004
0.006
0.008
q²(Å⁻²)
8355eV
8368eV
8370eV
8372eV
15.0 Å
Intensity
0
5
10
15
20
25
30
35
40
Degrees 2θ

Figure 5

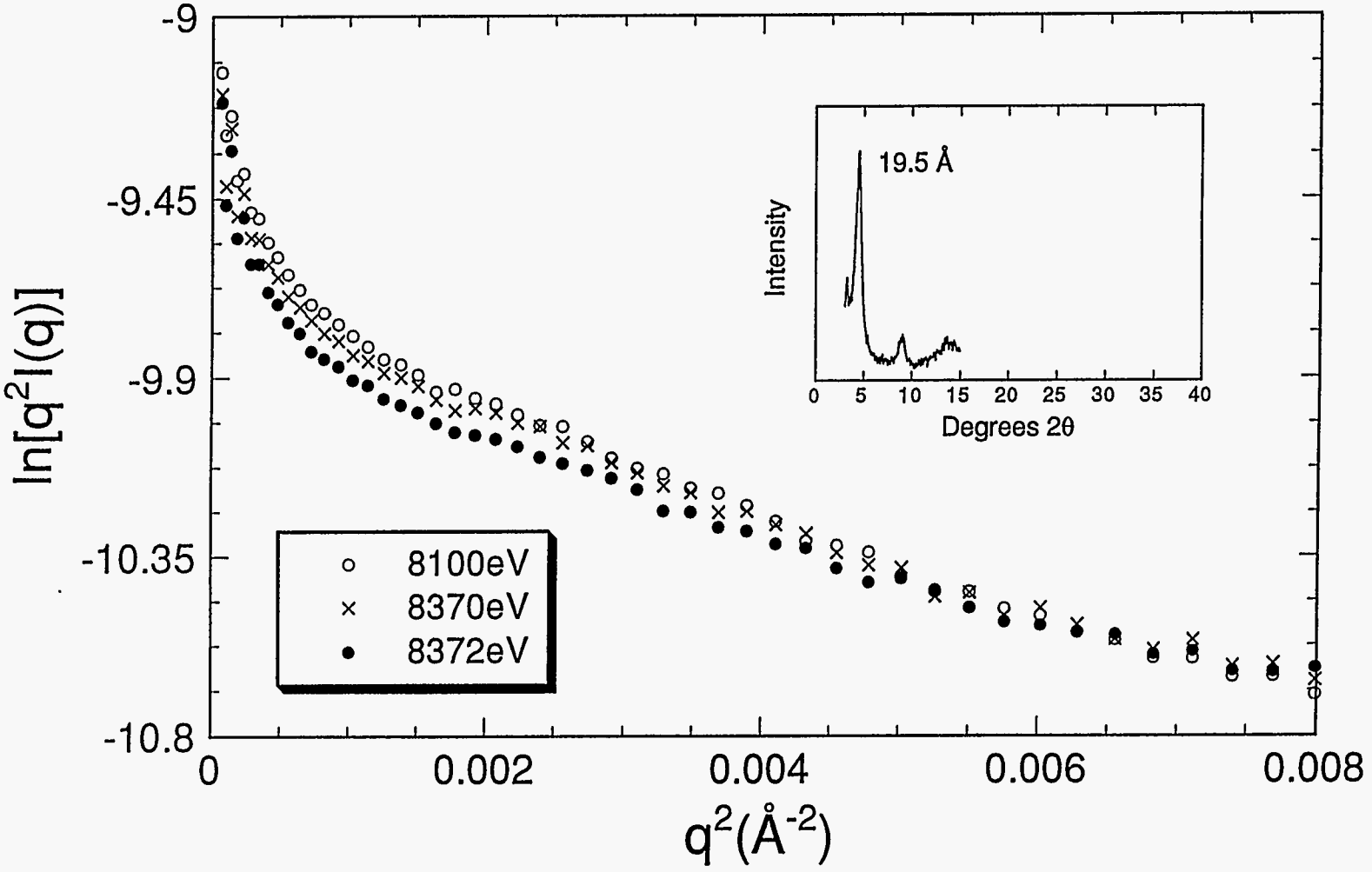
-9
-9.45
-9.9
-10.35
-10.8
ln[q²I(q)]
0
0.002
0.004
0.006
0.008
q²(Å⁻²)
8100eV
8370eV
8372eV
19.5 Å
Intensity
0
5
10
15
20
25
30
35
40
Degrees 2θ

Figure 6